

Computational and Experimental Procedures for the Structural Integrity Analysis

Miklós János PRODÁN

Institute of Materials Science and Technology (ATT)

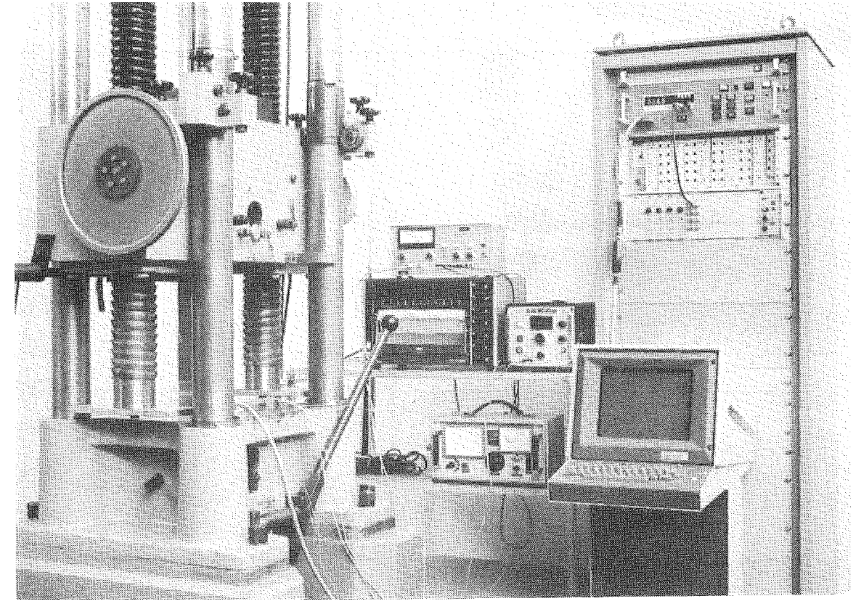
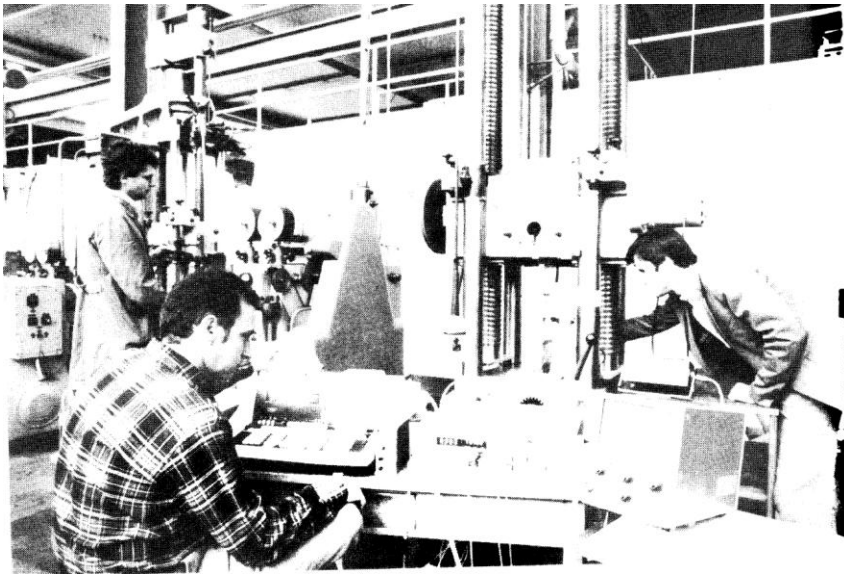
Faculty of Mechanical Engineering

Budapest University of Technology and Economy (BME)

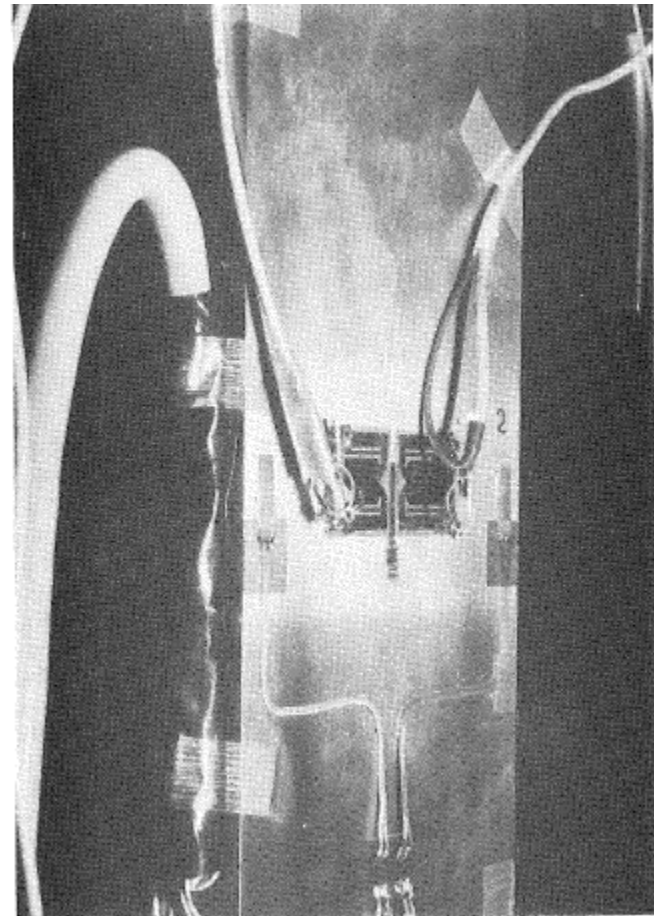
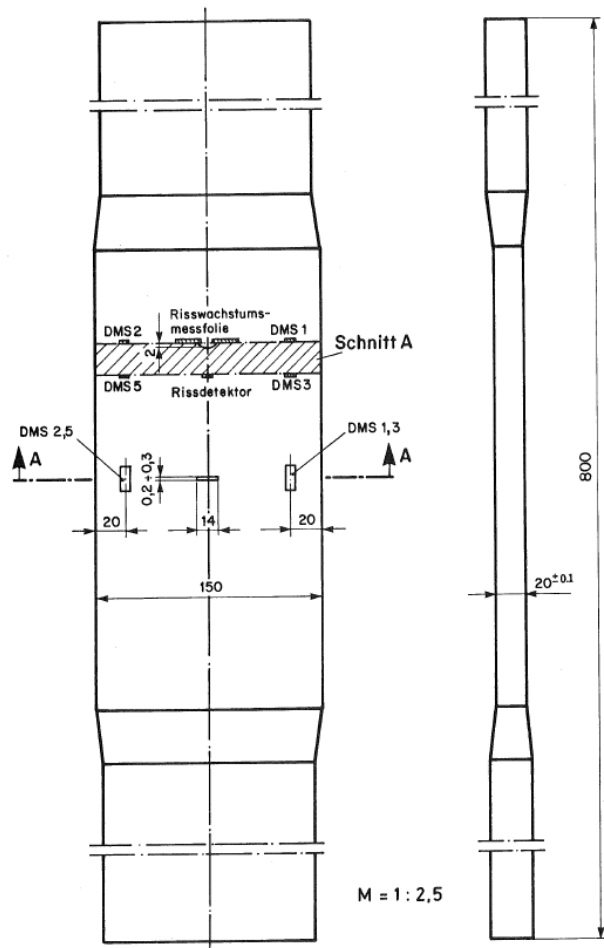
Contents

- Experiments (fatigue life)
- Computations (fatigue life)
- The result: A semi-empirical /semi-computational procedure
- Medical Technology – Tasks: Stents, Balloon dilatation catheters, Dental implants

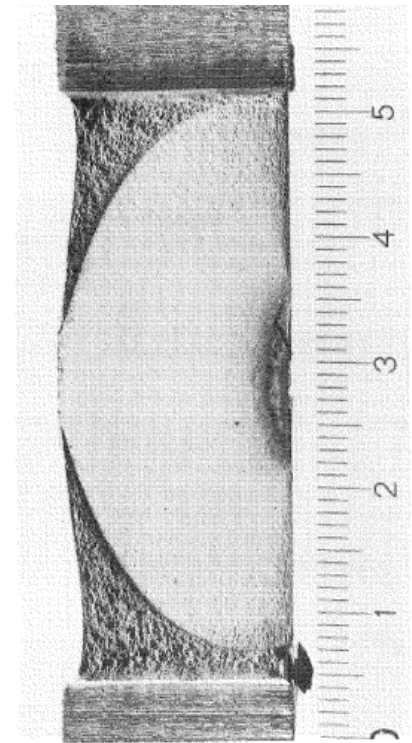
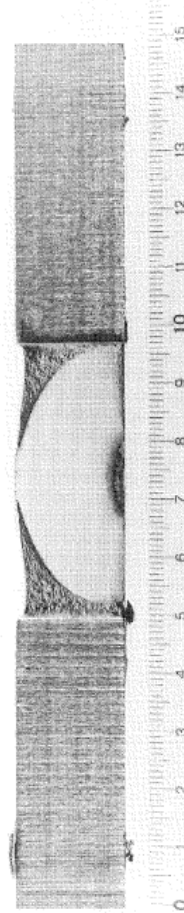
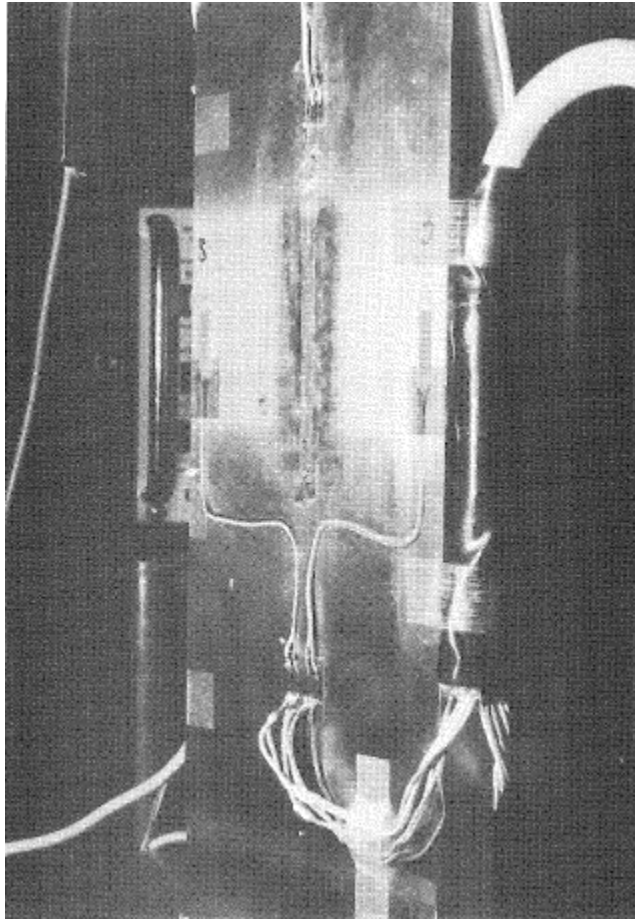
The experimental setup with tensile plate specimens



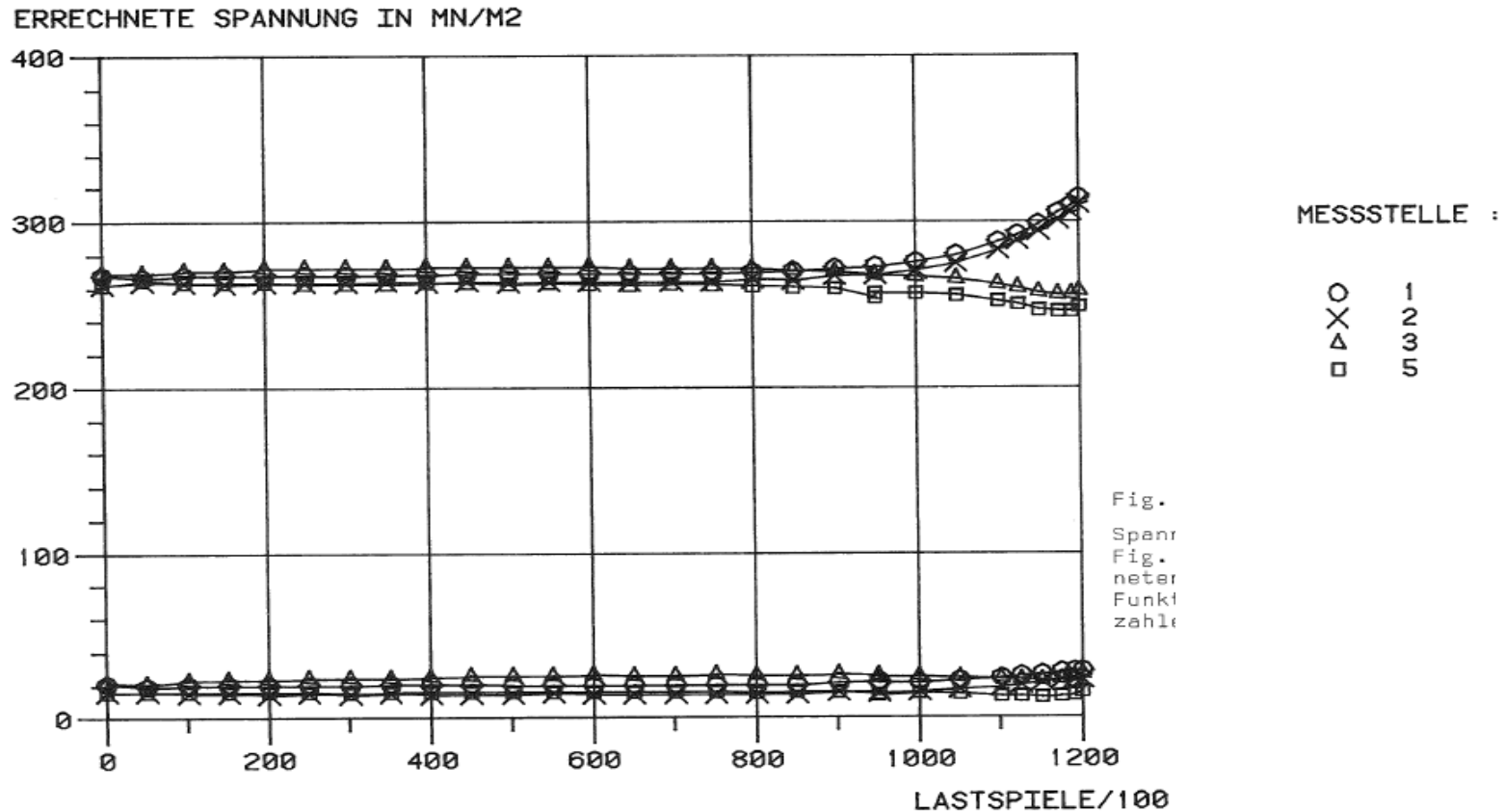
The technical drawing of the plate and a photo frontwise



The backside and fatigue fracture surfaces after the test (leak-before-break in case of a pressure vessel)



Sinusoidal cyclic loading with $\Delta\sigma=250$ MPa, signals from the four strain-gauges Nr. 1,2 and 3,5 (after 100'000 cycles little bending effects)



A pressure vessel with a flaw – our tensile plate can be looked at as a model for this practical application

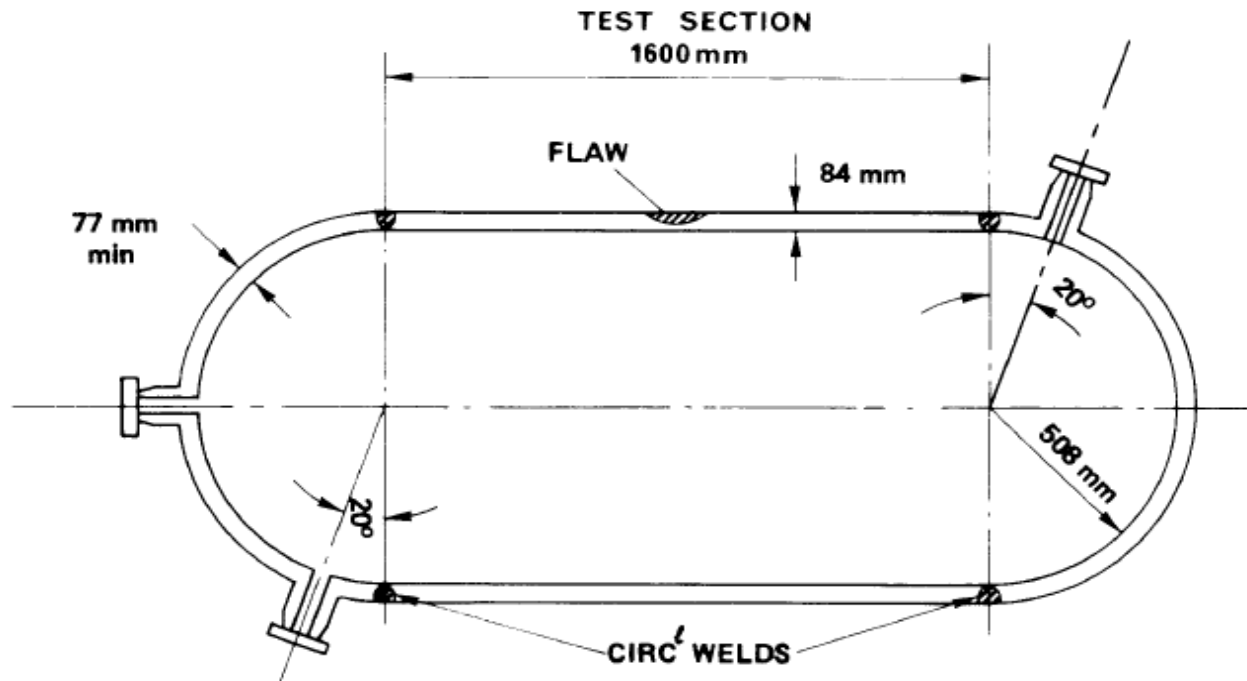
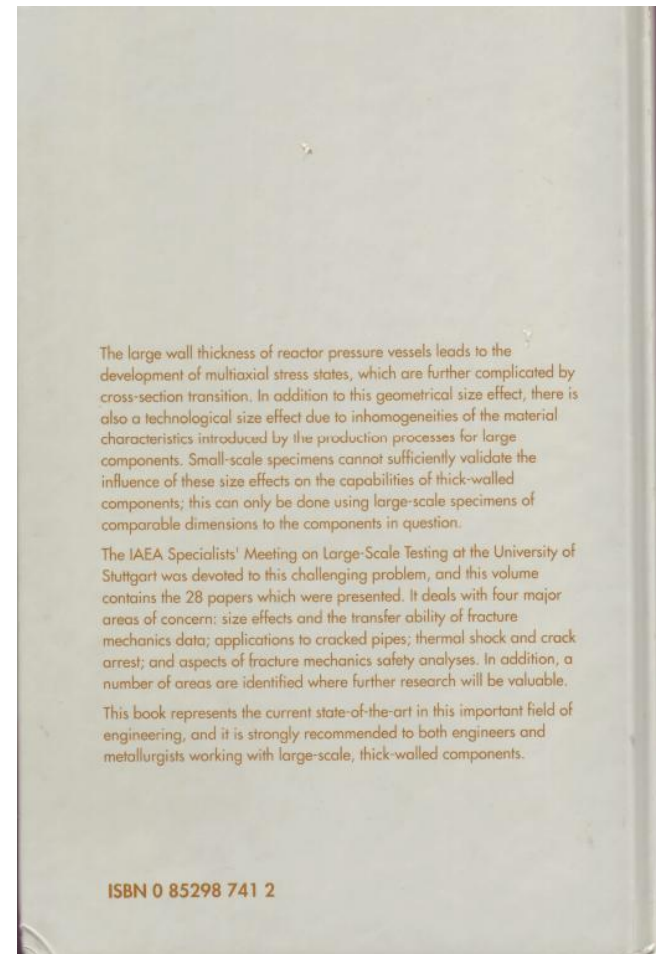
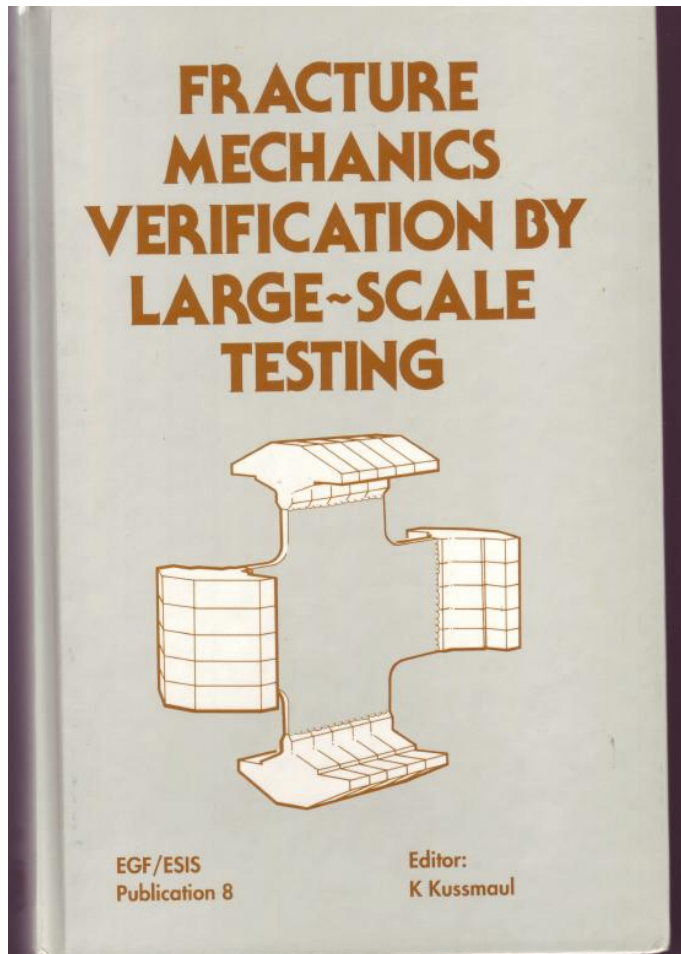


Fig 2 Geometry of CEGB pressure vessel test 1

CEGB= Central Electricity Generating Board, London (U.K.)

Cover (frontpage and backpage) of the book containing firstly (in 1991) the results given in this presentation



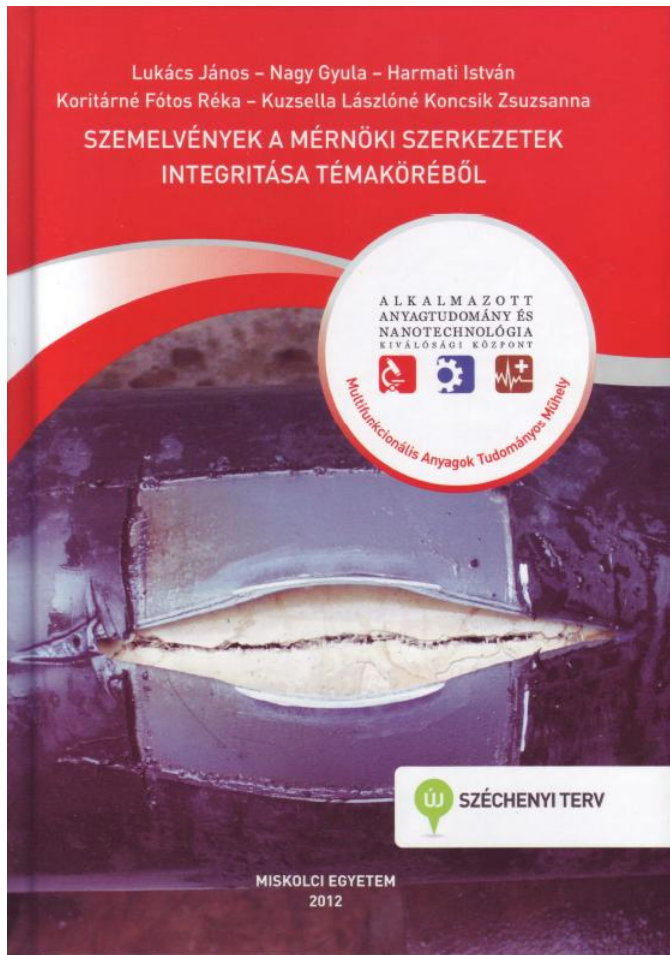
Experiments with part-through cracks of today (2015) - Project STYLE of the Bay Zoltán Nonprofit Ltd. for Appl. Research, Miskolc-Tapolca

STYLE= Structural integrity for lifetime
management – non-RPV



Thanks for these photos to Mr. Péter Rózsahegyi, Head
of Laboratory – Bay Zoltán Institute, Miskolc-Tapolca

Left: Research at the Institute of Structural Integrity, Director: Prof. Dr. LUKÁCS János, Miskolc University, Cover: Pipe Rupture

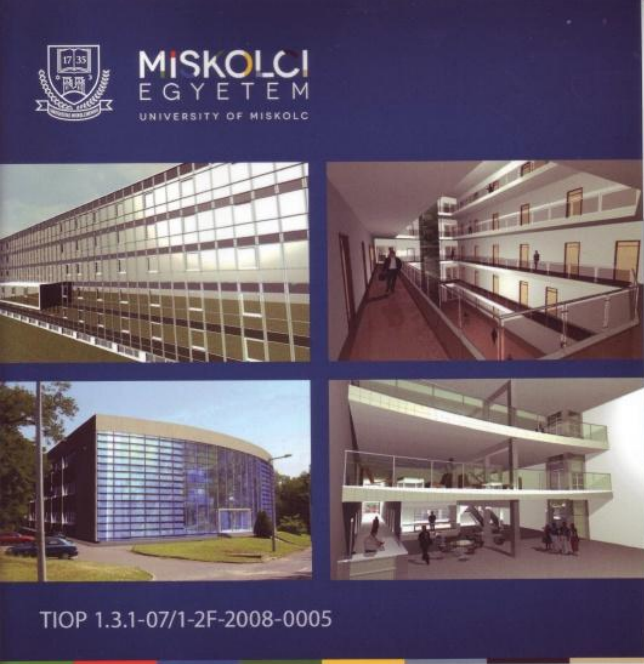


42nd Seminar of HKTCC

Dr. Prodán M. J.: On the Structural Integrity of Machine Elements and Engineering Structures

Hotel Gellért, Budapest, 26th October 2015

Prof. Lukács J. was also the manager of the rejuvenation of the campus. Costs: 7'000'000'000 HUF, finished 2015



MISKOLCI EGYETEM
UNIVERSITY OF MISKOLC

TIOP 1.3.1-07/1-2F-2008-0005

A Miskolci Egyetem hazai és nemzetközi versenyképességének komplex megújítása

TIOP 1.3.1-07/1-2F-2008-0005

MISKOLCI EGYETEM

A PROJEKT MENEDZSMENTJE

Projektvezető: Prof. Dr. Lukács János
Pénzügyi vezető: Szentirmai Zoltánné
Informatikai szakember: Illés Sándor
Projekt koordinátor: Lukácsné Huszti Mónika
Műszaki, építési szakember:
Bubnó László, majd Vilmos Zoltán
Projekt adminisztrátor: Barna Anita

KARI FELELŐSÖK

MŰSZAKI FÖLDTUDOMÁNYI KAR
eszközbeszerzés:
Dr. Ormos Tamás, majd Dr. Debreczeni Ákos
építés, felújítás: Dr. Gombkötő Imre
MŰSZAKI ANYAGTUDOMÁNYI KAR
eszközbeszerzés: Prof. Dr. Mertinger Valéria
építés, felújítás: Ferenczi Tibor
GÉPÉSZMÉRNÖKI ÉS INFORMATIKAI KAR
eszközbeszerzés: Dr. Kalmár László,
majd Dr. Németh János
építés, felújítás: Korpás Kálmán,
majd Dr. Barna Balázs, Wágner György
GAZDASÁGTUDOMÁNYI KAR
Dr. Szakály Dezső,
majd Dr. Nagy Zoltán
COMENIUS FŐISKOLAI KAR
Szentirmai László, majd Dr. Nagy György
és Kántor Istvánné
ALKALMAZOTT FÖLDTUDOMÁNYI KUTATÓINTÉZET
eszközbeszerzés: Dr. Jónap Károly
építés, felújítás: Vörös Csaba
SZÁMÍTÓKÖZPONT
eszközbeszerzés: Illés Sándor
építés, felújítás: Varga László

PROJEKT WEBLAP

<http://www.uni-miskolc.hu/uni/dept/TIOP/>
Dr. Vitéz Gáborné és Veréb Norbert

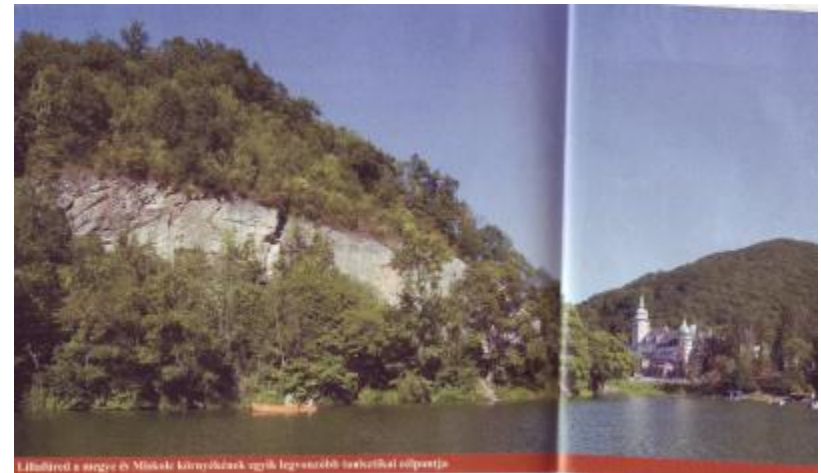
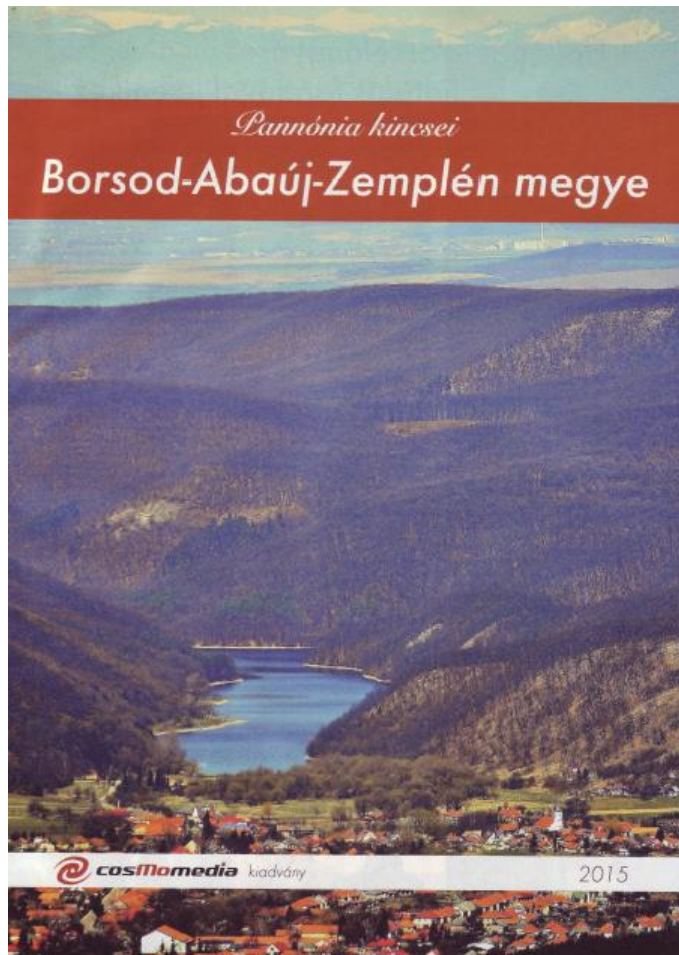
KÖZBESZERZÉS

Közbeszerzéseket Előkészítő Bizottság (KEB):
Dr. Biróné dr. Vajnorák Zsuzsanna
Közbeszerzési Tanács (KT)

MŰSZAKI TÁMOGATÁS

Műszaki és Üzemeltetési Főosztály:
Rutkai János, majd Molnár Miklós
később
Üzemeltetési Igazgatóság: Pintér Zoltán

The surrounding of Miskolc, „capital“ of North-Hungary, with the University and Bay Zoltán Inst. as „Genius loci“



Computations, verified by the experiments shown above. The computational model for the plate with appropriate notations

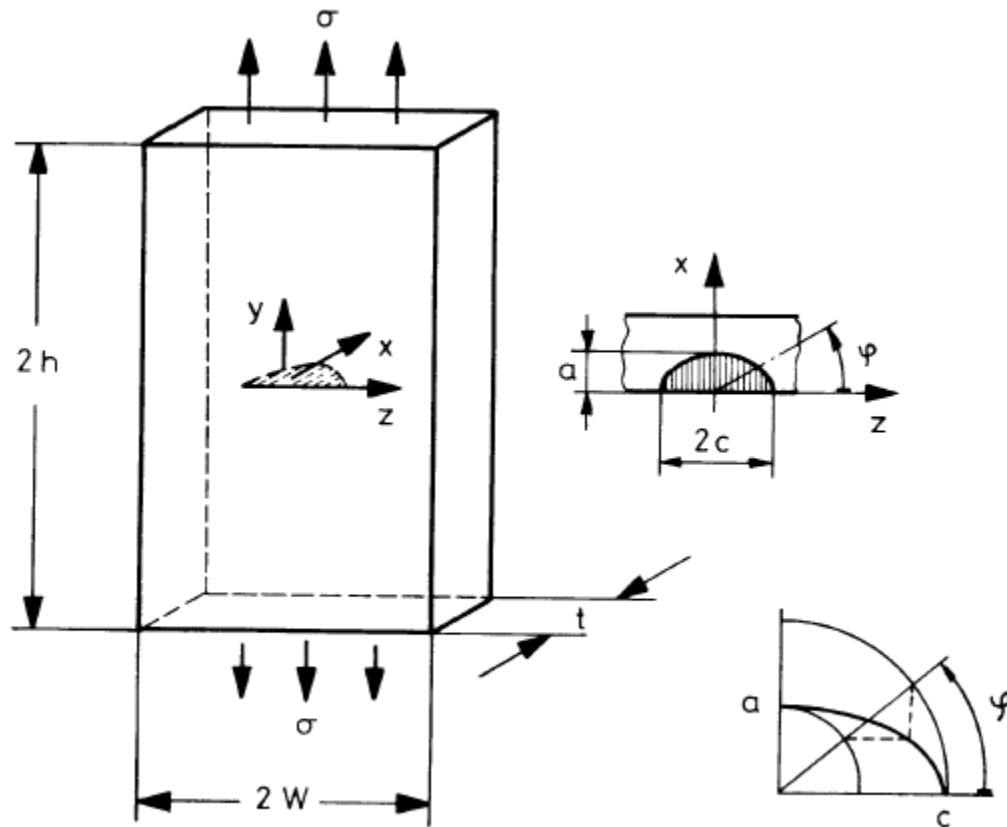


Fig 2 Surface crack in a tensile plate

Explanations of the stepwise computation of fatigue crack growth – Equation (2), see on this slide

(a) Calculation of the crack half length c_i

$$c_i = c_{i-1} + (a_i - a_{i-1}) \left(\frac{a_{i-1}}{c_{i-1}} \right)^{m/2} \quad (2)$$

from the known crack depth a_i and the results of the previous step, c_{i-1} and a_{i-1} , using a material-dependent exponent $m/2$ ($2 < m < 5$, e.g., $m = 3$).

According to Raju and Newman, the stress intensity factor, K , is

$$K = \frac{\sigma \sqrt{(\pi a)}}{\Phi} F\left(\frac{a}{c}, \varphi, \frac{a}{t}\right) \quad (5)$$

where

$$c/W \leq 0.25$$

and

$$c/h \leq 0.25$$

The correction factors

$$F\left(\frac{a}{c}, \varphi, \frac{a}{t}\right) = \frac{K \cdot \Phi}{\sigma \sqrt{(\pi a)}} \quad (6)$$

are given in Table 1.

Finite Element Results of Raju & Newman (NASA) for the Correction Factors in Equation (5) of the previous slide

Table 1 Correction factors $F(a/c, \phi, a/t)$ from reference (1)

a/c	a/t	ϕ (degrees)								
		0.00	11.25	22.50	33.75	45.00	56.25	67.50	78.75	90.00
0.20	0.20	0.617	0.650	0.754	0.882	0.990	1.072	1.128	1.161	1.173
0.40	0.20	0.767	0.781	0.842	0.923	0.998	1.058	1.103	1.129	1.138
0.60	0.20	0.916	0.919	0.942	0.982	1.024	1.059	1.087	1.104	1.110
1.00	0.20	1.174	1.145	1.105	1.082	1.067	1.058	1.053	1.050	1.049
2.00	0.20	0.821	0.749	0.740	0.692	0.646	0.599	0.552	0.512	0.495
0.20	0.40	0.724	0.775	0.883	1.009	1.122	1.222	1.297	1.344	1.359
0.40	0.40	0.896	0.902	0.946	1.010	1.075	1.136	1.184	1.214	1.225
0.60	0.40	1.015	1.004	1.009	1.033	1.062	1.093	1.121	1.139	1.145
1.00	0.40	1.229	1.206	1.157	1.126	1.104	1.088	1.075	1.066	1.062
2.00	0.40	0.848	0.818	0.759	0.708	0.659	0.609	0.560	0.519	0.501
0.20	0.60	0.899	0.953	1.080	1.237	1.384	1.501	1.581	1.627	1.642
0.40	0.60	1.080	1.075	1.113	1.179	1.247	1.302	1.341	1.363	1.370
0.60	0.60	1.172	1.149	1.142	1.160	1.182	1.202	1.218	1.227	1.230
1.00	0.60	1.355	1.321	1.256	1.214	1.181	1.153	1.129	1.113	1.107
2.00	0.60	0.866	0.833	0.771	0.716	0.664	0.610	0.560	0.519	0.501
0.20	0.80	1.190	1.217	1.345	1.504	1.657	1.759	1.824	1.846	1.851
0.40	0.80	1.318	1.285	1.297	1.327	1.374	1.408	1.437	1.446	1.447
0.60	0.80	1.353	1.304	1.265	1.240	1.243	1.245	1.260	1.264	1.264
1.00	0.80	1.464	1.410	1.314	1.234	1.193	1.150	1.134	1.118	1.112
2.00	0.80	0.876	0.839	0.775	0.717	0.661	0.607	0.554	0.513	0.496

Some additional ideas to Equation (2) with the Equations (3) and (4) /Irwin/ and (5) /Paris/

Formula (2) was deduced from equations established by Irwin (4) and Paris (5) in the following way.

Irwin's equation (4) is

$$K = \frac{\sigma\sqrt{(\pi a)}}{\Phi} \left\{ \left(\frac{a^2}{c^2} \right) \cos^2 \varphi + \sin^2 \varphi \right\}^{1/4} \quad (3)$$

where Φ is a complete elliptic integral of the second kind

$$\Phi = \int_0^{\pi/2} \left\{ \sin^2 \varphi + \left(\frac{a}{c} \right)^2 \cos^2 \varphi \right\}^{1/2} d\varphi \quad (4)$$

For the crack in c -direction and $\varphi = 0$ the K value is

$$K_0 = \frac{\sigma\sqrt{(\pi a)}}{\Phi} \cdot \left(\frac{a}{c} \right)^{1/2}$$

Similarly, for the crack in the a direction and $\varphi = \pi/2$

$$K_{\pi/2} = \frac{\sigma\sqrt{(\pi a)}}{\Phi}$$

Final steps of our deduction of Equation (2), necessary for the procedure firstly proposed in the PhD thesis of the author

Using the Paris equation (5) we obtain

$$\frac{\Delta c}{\Delta N} = C \cdot \Delta K_0^m$$

$$\frac{\Delta a}{\Delta N} = C \cdot \Delta K_{\pi/2}^m$$

Dividing the above expressions we have

$$\frac{\Delta c}{\Delta a} = \left(\frac{\Delta K_0}{\Delta K_{\pi/2}} \right)^m$$

and since, from equation (3)

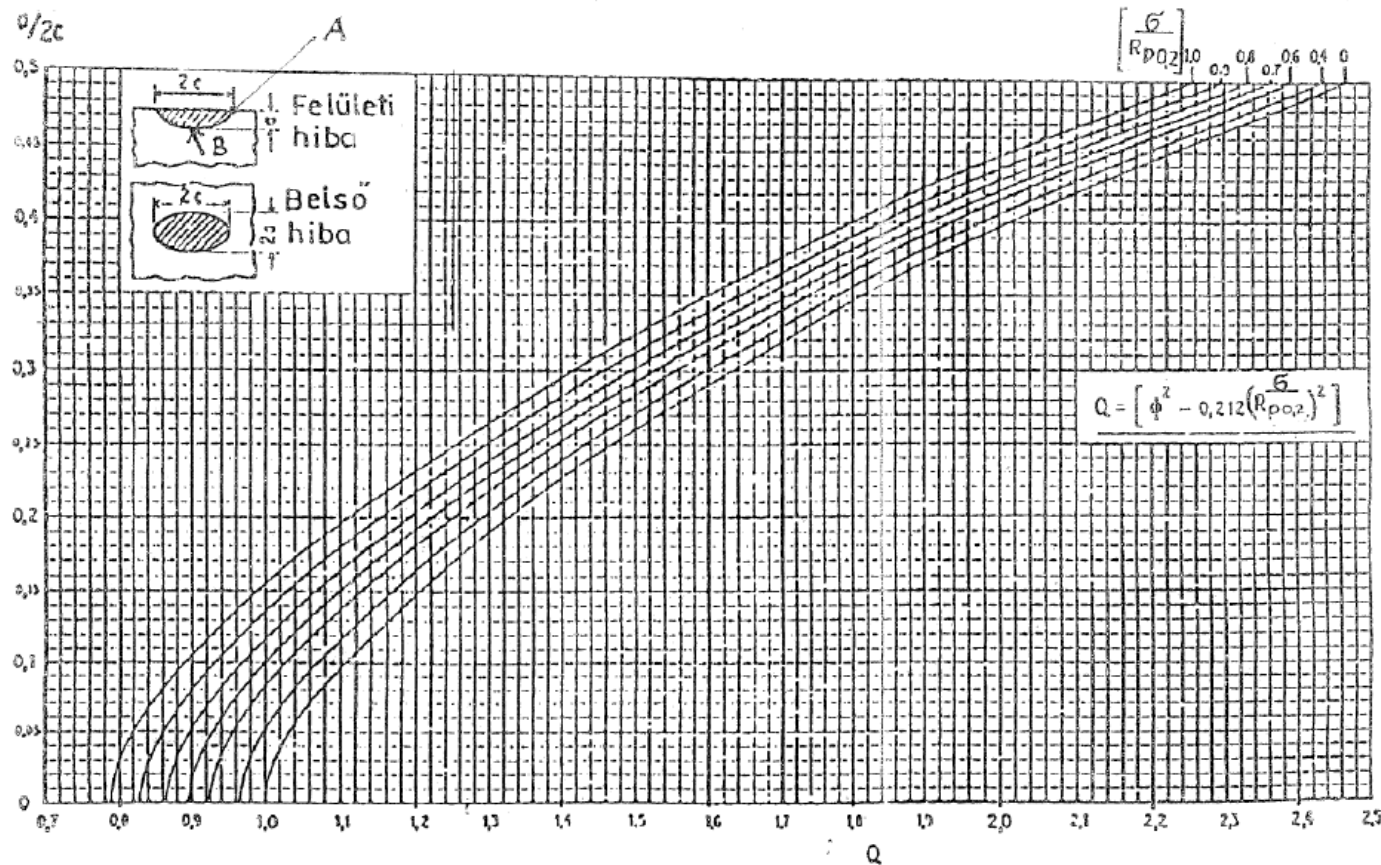
$$\frac{\Delta K_0}{\Delta K_{\pi/2}} = \left(\frac{a}{c} \right)^{1/2}$$

therefore

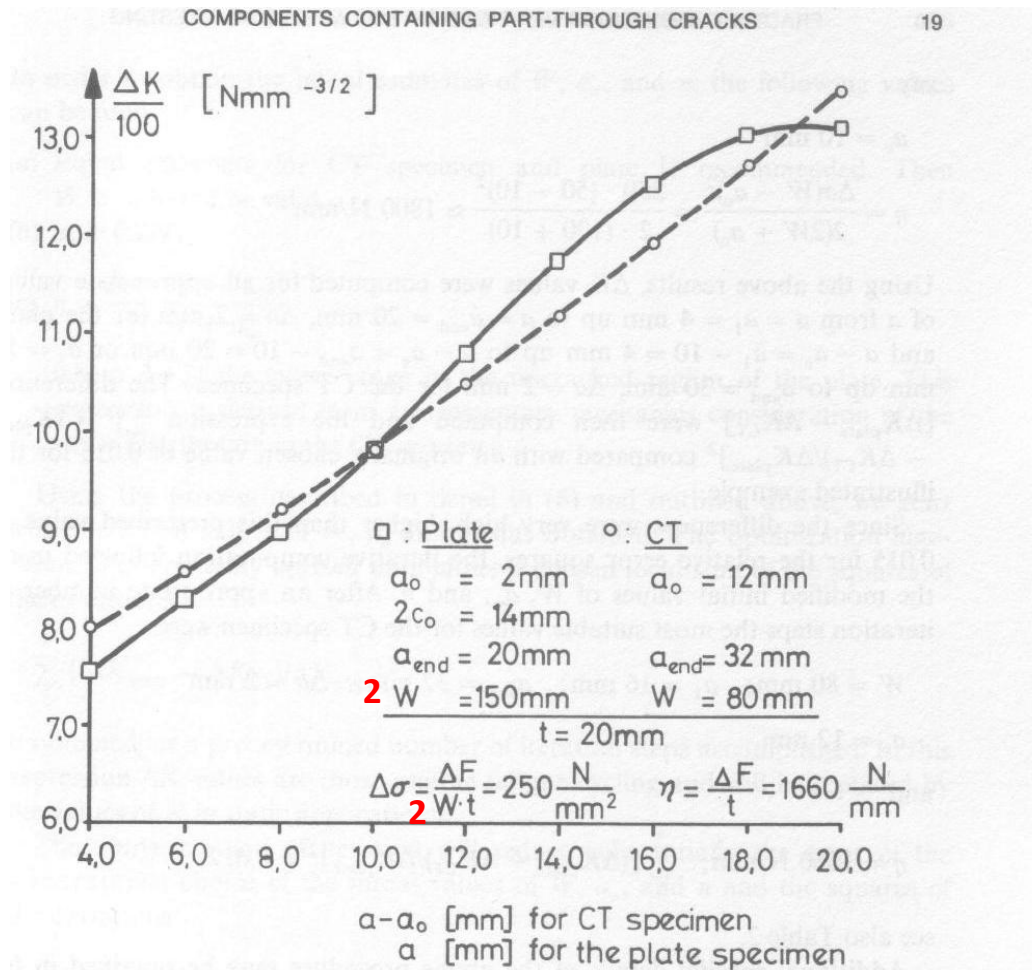
$$\frac{\Delta c}{\Delta a} = \left(\frac{a}{c} \right)^{m/2}$$

as shown rearranged in equation (2) with quoted indices.

A graphical illustration of the elliptic integral Φ of the second kind and of the crack shape factor Q



A numerical example: A tensile plate and a corresponding CT specimen with a growing crack (fatigue) from a_0 till a_{end}



Comments to the numerical computations

for a plate 150 mm wide, 20 mm thick and 800 mm long. The crack growth was divided into nine steps from $a_1 = 4$ mm to $a_{\text{end}} = 20$ mm when the crack reached the other side of the plate. All the steps are plotted in Fig. 3 as a full line.

Kapson minimization scheme were used in the following way. The growing crack shapes and the respective K values can be computed for the plate using equations (2) and (5). A typical example is shown in Fig. 3 (full line curve). Here the crack starter (spark eroded notch) was as follows

$$a_0 = 2 \text{ mm}$$

$$2c_0 = 14 \text{ mm}$$

Computation of Point P_3 ($a_3; \Delta K_3$), i.e. P_3 (8 mm; $\approx 900 \text{ Nmm}^{-3/2}$) of the earlier slide for the plate

1. Berechnung von c_3

$$c_1 = 7,305 \text{ mm} ; \quad c_2 = 8,12 \text{ mm} ; \quad c_3 = c_2 + (a_3 - a_2) \left(\frac{a_2}{c_2} \right)^{1,5} = 9,4 \text{ mm}$$

2. Berechnung von $F_3 \left(\frac{a_3}{c_3}, 90^\circ, \frac{a_3}{t} \right)$

$$\frac{a_3}{c_3} = \frac{8}{9,4} = 0,85 \quad \frac{a_3}{t} = \frac{8}{20} = 0,4 \quad F_3 = 1,093 \text{ interpoliert aus Tab. 1}$$

3. Berechnung von Φ (elliptisches Integral 2. Art)

$$\frac{a_3}{2c_3} = \frac{8}{18,8} = 0,426$$

$$\text{Ablesewert: } Q = 2,14 \rightarrow \Phi = \sqrt{Q} = \sqrt{2,14} = 1,462$$

Computation of Point P₃ (a₃; ΔK₃), i.e. P₃ (8 mm; ≈900 Nmm^{-3/2}) of the earlier slide for the plate
Computation continued

4. Berechnung von ΔK₃

$$\Delta K_3 = \frac{250 \cdot \sqrt{\pi \cdot 8}}{1,462} \cdot 1,093 = 937 \text{ Nmm}^{-3/2}$$

$$\text{Fehler} = \frac{937 - 900}{900} \approx 4 \%$$

Fehler, verglichen mit dem Wert in EMPA Bericht Nr. 213 , S. 41

$$\text{Fehler} = \frac{937 - 923}{923} \approx 1,5 \%$$

All numerical values illustrated in the earlier slide

FRACTURE MECHANICS VERIFICATION BY LARGE-SCALE TESTING

Table 2 Tabulated results illustrated in Fig. 3

$a - a_0$ (mm) CT specimen	ΔK ($N\ mm^{-3/2}$)	
a (mm) plate	plate	CT specimen
4	752	797
6	833	857
8	898	919
10	982	983
12	1079	1050
14	1174	1120
16	1254	1195
18	1304	1275
20	1308	1362

Tensile plates experimental results with four plates

FRACTURE MECHANICS VERIFICATION BY LARGE-SCALE TESTING

Table 3 Tensile plates experimental results

a (mm)	N	c (mm)	a (mm)	N	c (mm)
<i>Plate specimen No. 1</i>			<i>Plate specimen No. 3</i>		
1.79	0	7.00	1.61	0	7.00
2.24	10 000	7.00	1.73	3000	7.00
2.84	20 000	7.00	2.01	10 000	7.00
3.57	30 000	7.15	2.43	20 000	7.00
4.49	40 000	7.50	2.91	30 000	7.00
4.93	45 000	7.70	3.33	40 000	7.00
6.79	60 000	9.10	3.62	50 000	7.00
7.48	65 000	9.85	3.92	60 000	7.05
8.68	70 000	10.55	4.35	70 000	7.20
10.03	75 000	11.95	5.20	80 000	7.45
11.62	80 000	13.35	6.86	90 000	8.25
13.50	85 000	15.20	9.51	100 000	9.90
14.18	87 000	16.60	13.48	110 000	13.30
14.58	88 000	17.80	16.21	115 000	16.20
15.53	90 000	18.80	17.49	117 000	17.35
16.36	91 400	19.45	18.85	119 000	19.60
17.07	92 500	20.80	19.56	120 000	20.95
18.32	94 300	22.70			
<i>Plate specimen No. 2</i>			<i>Plate specimen No. 4</i>		
2.13	0	7.00	1.95	0	7.00
2.31	10 000	7.00	2.14	10 000	7.00
2.83	20 000	7.00	2.58	20 000	7.00
3.68	30 000	7.00	3.28	30 000	7.00
4.74	40 000	7.05	4.34	40 000	7.00
6.33	50 000	7.45	5.10	50 000	7.20
8.33	60 000	8.70	6.20	60 000	7.60
10.99	70 000	10.65	8.04	70 000	9.20
14.87	80 000	14.25	10.68	80 000	11.40
16.69	84 000	16.95	15.28	90 000	15.50
17.86	86 000	17.75	15.65	90 500	16.80
18.78	87 500	18.80	16.70	92 500	17.60
20.08	89 500	20.95	18.42	94 000	18.40
			18.34	95 000	18.95
			18.48	96 000	19.60
			18.79	97 000	20.40
			18.94	97 500	20.80
			19.23	98 500	21.50

Graphical illustration of the tabulated results (see the Tables on the previous and on the following slide)

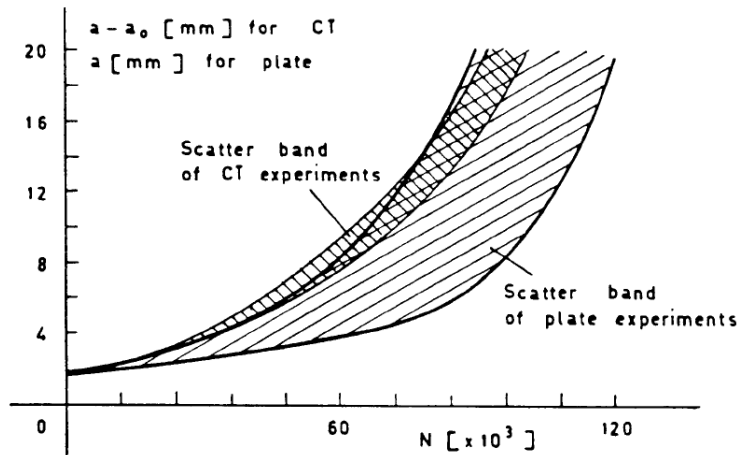


FIG. 4a—Crack propagation in tension plates and optimally adjusted C(T) specimens.

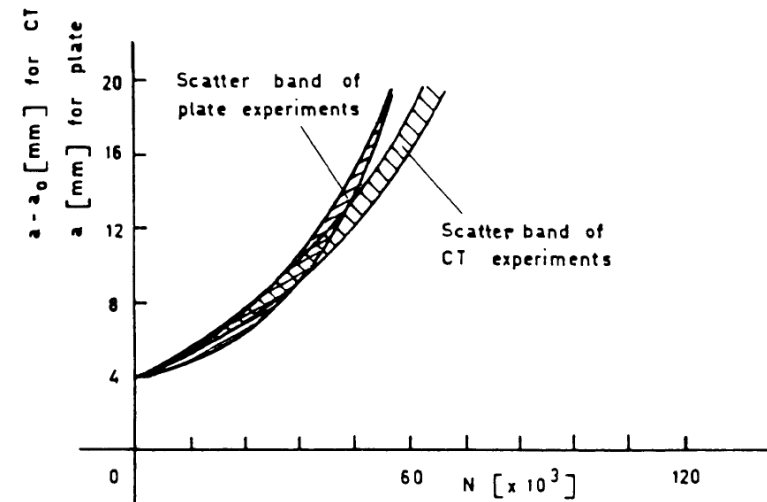


FIG. 4b—Transformations of crack growth curves (see Fig. 4a) to the origin at $N = 0$ and crack depth of 4 mm.

Experimental results with three adjusted CT specimens

TABLE 4—Experimental results for three adjusted C(T) specimens (see also Figs. 3 and 4a).

$(a - a_0)$, mm	N		
	No. 1	No. 2	No. 3
3.0	24 000	24 000	24 000
3.5	28 470	30 575	30 475
4.0	29 510	35 550	35 175
4.5	31 950	40 300	39 250
5.0	35 640	43 825	43 175
5.5	40 775	47 275	46 775
6.0	42 050	50 375	50 150
6.5	45 020	53 500	53 550
7.0	47 500	56 700	56 175
7.5	51 955	59 150	59 025
8.0	53 235	61 875	61 825
8.5	56 705	64 275	64 475
9.0	57 875	66 875	66 975
9.5	60 390	69 150	69 450
10.0	61 855	71 225	71 675
10.5	65 045	73 625	73 725
11.0	66 150	75 575	75 850
11.5	68 790	77 600	77 700
12.0	70 200	79 500	79 200
12.5	72 755	81 275	81 225
13.0	73 830	82 950	82 800
13.5	76 035	84 800	84 625
14.0	77 670	86 275	86 300
14.5	79 205	87 800	87 725
15.0	79 935	89 350	89 175
15.5	81 230	90 900	90 625
16.0	82 175	92 275	91 925
16.5	84 010	93 575	93 300
17.0	84 800	94 850	94 625
17.5	86 240	96 000	95 800
18.0	87 320	...	96 900
18.5	88 370	...	98 025
19.0	89 305

Some additional results from the research work „dealing with semielliptical surface cracks“

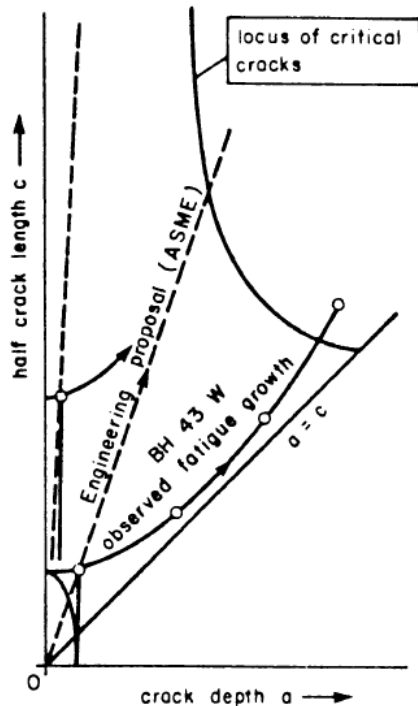


FIG. 5—Fatigue growth of surface cracks towards critical size. Comparison of experimental results with ASME Code, Section XI.

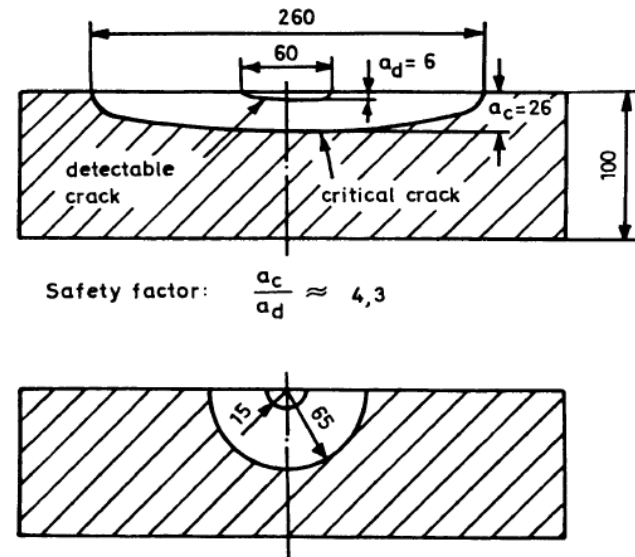


FIG. 6—Two examples of critical and detectable crack sizes: (a) semi-elliptical and (b) semicircular cracks.

Conclusions of Part I: Semielliptical surface cracks

- Our research work verified the hypothesis that two-dimensional surface crack growth in a vessel wall is controlled by ΔK in the same way as a quasi one-dimensional straight-fronted crack growth in a CT specimen (plane strain, plane stress or intermediate conditions)
- Optimally corresponding CT specimens to a vessel (or CCT: center-cracked tensile plate) application – adjusted with the new proposal – can be better used for fatigue life time predictions than earlier experiments without this adjustment or optimization

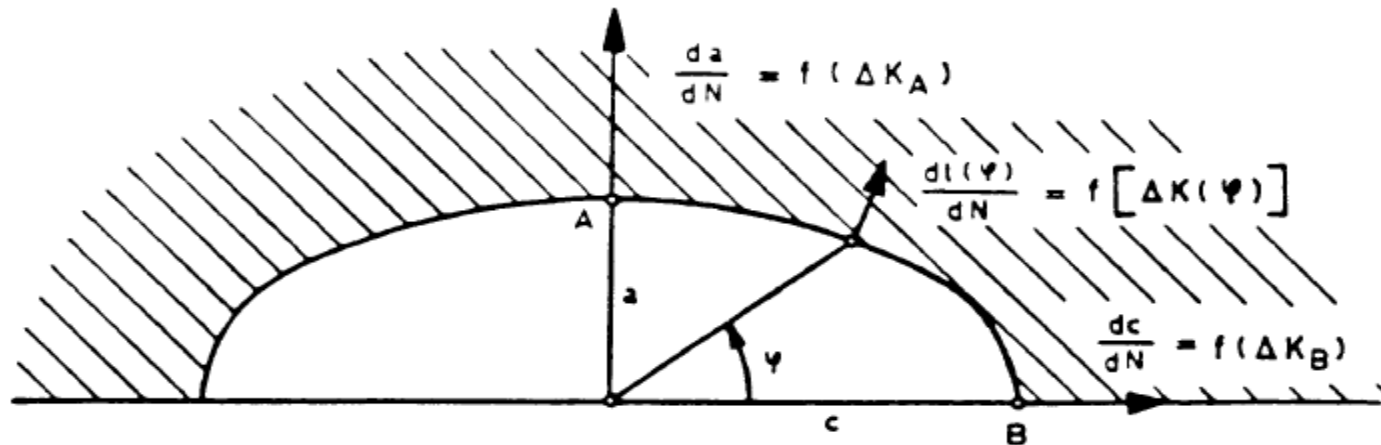


FIG. 1—Fatigue crack growth of a surface crack in isotropic material (resistance to crack propagation is considered to be independent of direction).

Two actualities in Swiss nuclear power plants (Beznau and Leibstadt) in Juni 2014 and October 2015

Bericht zu Leck im AKW Beznau

(sda) · Wegen Reparaturarbeiten musste der Block 1 des AKW Beznau im Kanton Aargau Ende Juni während zweier Wochen abgeschaltet werden. Bei einem Rundgang war im Rücklauf des primären Nebenkühlwassersystems eine geringfügige Leckage festgestellt worden. Die Aufsichtsbehörde Ensi hat nun einen Bericht dazu vorgelegt. Sie kommt zum Schluss, dass das Vorkommnis eine geringe Bedeutung für die nukleare Sicherheit gehabt habe. Die Hauptursache für die Rissbildung bei einer Rücklaufleitung seien hochfrequente Schwingungen gewesen. Als Konsequenz forderte die Aufsichtsbehörde weitere Analysen in Hinblick auf ähnlich positionierte Leitungen im primären Nebenkühlwasserkreislauf.



Neue Zürcher Zeitung

Defekt im Kühlkreislauf

AKW Leibstadt abgeschaltet

Das Atomkraftwerk Leibstadt im Kanton Aargau ist am Samstag vom Netz genommen worden. Grund dafür ist ein Defekt im Kühlwasserkreislauf des Generator-Stators. Wie lange das AKW abgeschaltet bleibt, ist zunächst unklar.

17.10.2015, 12:27 Uhr 4 Kommentare

(sda) Das AKW wurde kurz nach 11 Uhr vom Netz getrennt, wie die Kernkraftwerk Leibstadt (KKL) am Samstag mitteilte. Das sei notwendig gewesen, um die Inspektion am Generator vornehmen und den Defekt lokalisieren zu können

Der Generator verfügt über zwei Kühlkreisläufe, einer für den sogenannten Stator und einer für den Rotor. Während der Rotor mit Wasserstoff gekühlt wird, benötigt der Stator eine konventionelle Wasserkühlung. Dieser Teil der Anlage hat keinen Zusammenhang zum nuklearen Teil.

Tasks on the topic of Medical Technology at ATT BME

- Balloon dilatation catheters
- Stents
- Dental implants

2014 Annual Meeting of the Swiss Material Testing Society
(SVMT) at Biotronik Ltd., Bülach (Kt. Zürich / Switzerland)
Main theme: Medical Technology



From Prof. Grüntzig, Zürich till ATT Budapest

- [Andreas-Grüntzig-Forschungspreis](#)
- Die Auslobungsfrist ist der **31. Oktober 2015!**
- **Prof. Dr. Andreas Roland Grüntzig** wurde am 25. Juni 1939 in Dresden geboren. Sein Vater fiel 1945 im Krieg. Nach dem Abitur in Leipzig nahm er 1958 das Medizinstudium in Heidelberg auf.
- Es folgten Assistentenjahre bei Prof. Ratschow (Darmstadt), Prof. Hegglin und Prof. Bollinger (Zürich), bei Prof. Siegenthaler in Innerer Medizin und Prof. Wellauer im Röntgendiagnostischen Zentralinstitut sowie später bei den Professoren Krayenbühl und Rutishauser in Zürich.
- **Im Jahre 1974 erfolgte die erste Ballondilatation einer Beinarterie am Menschen.** Als Oberarzt führte Prof. Grüntzig bereits 1975 tierexperimentelle Untersuchungen zur Koronardilatation durch. Die erste intraoperative Koronardilatation nahm er in San Francisco bei Prof. R. Myler vor.
- **Die inzwischen historische erste Ballondilatation eines Koronargefäßes am Menschen führte Prof. Grüntzig am 16. September 1977 in Zürich durch. Er eröffnete damit der interventionellen Kardiologie und speziell der Revaskularisation der Koronarien eine neue Dimension, die ihn weltbekannt machte. Die neue Therapieoption erfuhr eine beispiellose Resonanz und führte zu einem grundlegenden Strukturwandel der Kardiologie.**
- Von 1980 an war Prof. Grüntzig als Professor für Medizin und Radiologie sowie als Direktor der Interventionellen Kardiovaskulären Abteilung der Medizinischen Fakultät der Emory Universität in Atlanta, GA, U.S.A. tätig.
- Am 27. September 1985 wurde er Opfer eines Flugzeugabsturzes in den USA. Sein Lebensmotto lautete: „Ich habe mein Leben den Gefäßen gewidmet.“

Periodica Polytechnica
Mechanical Engineering

Visibility of Balloon
Dilatation Catheters

59(1), pp. 39-42, 2015

DOI: 10.3311/PPme.7832

Creative Commons Attribution ©

Liza Pelyhe¹*, Eszter Bognár^{1,2}

RESEARCH ARTICLE

Received 23 November 2014; accepted after revision 19 December 2014

Abstract

In this study, an easy to use measurement method was developed to quantify the balloon dilatation catheter visibility, thus making them comparable. The visibility of the distal and proximal markers and the balloon (average values of the markers) was determined for fourteen balloons of the same type and material, but different lengths and diameters. Repeatability of these values was tested by one volunteer and reproducibility by two volunteers: three times each for all the balloons used for the study. It was found that the average visibility for balloons was 12±2%, 13±2% for distal markers, and 13±2% for proximal markers. Values of distal and proximal markers did not represent significant difference ($p=0.20$). There was no significant difference determined for repeatability and reproducibility either (p values were between 0.71-0.93). Hence, the developed measurement method was repeatable and reproducible making it suitable for comparison of the balloon dilatation catheters based on visibility.

Keywords

balloon dilatation catheter, radiodetectability, visibility

1 Introduction

Cardiovascular diseases are the number one cause of death worldwide. 41% of death is caused by ischaemic heart disease and 35% by stroke [1]. These emergencies are caused by stenosis or occlusion of the vessels in the heart or brain [2]. One of the potential medical devices used for the dilatation of the vascular system is the balloon dilatation catheter [3].

The balloon dilatation catheter (so called balloon catheter [4-5]) is an intravascular catheter (single or multilumen tube), on which a balloon is located near the distal end (this end is introduced into the body). The hydraulic dilatation of this balloon dilates the narrowed, occluded vessel [3,6,7]. The balloon is monitored in the body using X-ray fluoroscopy [9-10].

The current standard for balloon dilatation catheters (ISO 10555-1:2013, ISO 10555-4:2013) and the guide of the U.S. Food and Drug Administration (FDA) specify that the balloon shall be radio-detectable when it is inserted into the body [3,6,11]. The placement of the balloon to the target place in the patient's vasculature is facilitated with radiopaque material. This radiopaque material is typically a metal marker band. It may be placed on the centre of the balloon (single metal marker) or on the ends of the balloon (double metal marker) [12,13].

In the standard for general requirements of the intravascular catheters (ISO 10555-1:2013), Part 4 relates to the balloon dilatation catheters, and requests the test method of visibility according to the standard ASTM F640-12 [3,6,14]. It contains standard test methods for determining radiopacity however; it does not specify the type of the medical devices. The guide of the FDA indicates that the radiopaque markers on the balloon should be investigated [11,14,15], but unified measure method is not recommended in the standards and literature. The manufacturer can measure this visibility by different methods, therefore they are not comparable. The methods of the manufacturer are not available. According to the standard (ASTM F640-12) pixel density or optical density are determined by some method.

The measured visibility values are not quantified; instead of terms were used for visibility's characterization, such as: excellent [16], optimal radiopacity [17], optimal visibility [18], and increased radiopacity [19], extremely visible [20].

¹Department of Materials Science and Engineering, Faculty of Mechanical Engineering,

Budapest University of Technology and Economics,

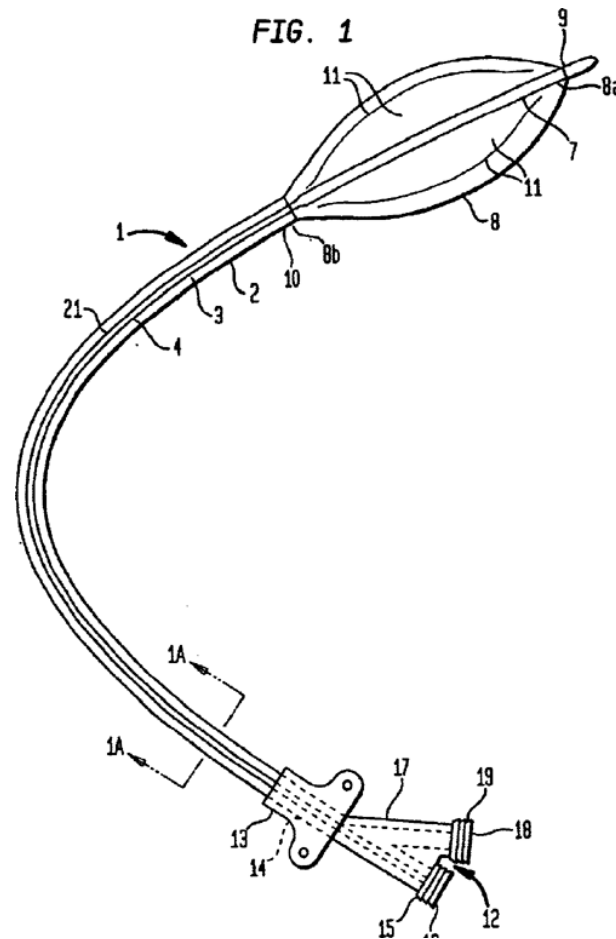
H-1111 Budapest, Bertalan Lajos u. 7, Hungary

²MTA-BME Research Group for Composite Science and Technology,

H-1111 Budapest, Műegyetem rkp. 3, Hungary

*Corresponding author, e-mail: liza@elk.bme.hu

A picture of a balloon dilatation catheter from Wikipedia (the Internet-Encyclopedia)





Thank you for your kind attention.